Frequency-dependent cavity lifetime and apparent superluminality in Fabry-Pérot-like interferometers

H. Y. Yao,[1] N. C. Chen,[1] T. H. Chang,[1,*] and H. G. Winful[2,†]

[1]*Department of Physics, National Tsing Hua University, No. 101, Section 2, Kuang-Fu Road, Hsinchu, Taiwan*

[2]*Department of Electrical Engineering and Computer Science, University of Michigan, 1301 Beal Avenue, Ann Arbor, Michigan 48109-2122, USA*

(Received 23 August 2012; published 28 November 2012)

Extraordinary group delays shorter than the transit time of light propagating at c through an equal distance have been experimentally demonstrated in single-Fabry-Pérot (FP) waveguide systems and cascaded-FP structures under off-resonant conditions. These "superluminal" phenomena are well explained by the multiple-reflection destructive interference that reduces the intracavity stored energy when operating off resonances. Excellent agreement between theory and experiment is obtained when the dispersive effects of reflective boundaries are considered. These results provide further insight into the nature of apparent superluminality in regions of allowed propagation.

DOI: 10.1103/PhysRevA.86.053832 PACS number(s): 42.25.Bs, 41.20.−q, 03.65.−w, 03.50.De

I. INTRODUCTION

Extraordinary group delays (GD) for wave packets transmitted through various systems have stimulated interest in the understanding and applications of phenomena classified as "slow light" [1,2] and "superluminal propagation" [3–11]. Superluminality, featuring group delays shorter than the normal delay of light traveling with the vacuum speed c, has been attributed to two major mechanisms: tunneling [4–8] and steep anomalous dispersion [10,11]. In the 1960s, Hartman reported that the group delay for tunneling through a barrier would saturate with the increase of the barrier width [8], leading to the positive superluminality in the case of opaque-barrier tunneling. This prediction has been verified in numerous experiments [7,12,13]. Recently, the underlying physics of superluminal tunneling was explicitly studied by Winful under the quasistatic condition [14–16], i.e., the spatial width of the wave packet should be much wider than the barrier width. The group delay in single-barrier tunneling was decomposed into a dwell time and a self-interference time [15–17], which are associated with the field energy storage time in the barrier and the self-interference process in front of the barrier, respectively. The theory was then applied to regions of allowed propagation, such as high-Q Fabry-Pérot (FP) cavities implemented by double-barrier systems, where a previously claimed lack of dependence of group delay on cavity length (the so-called generalized Hartman effect [6]) was shown to be a mere artifact [18]. In Ref. [18], it was assumed for simplicity that there is no dispersion in the amplitude and phase of the reflection and transmission coefficients of the cavity boundaries. This assumption makes the transmission group delay (Eq. (6) in Ref. [18]) exactly equal to the dwell time (Eq. (9) in Ref. [18]) under quasistatic condition and hence restricts the applicability of the theory.

This paper follows the work of Ref. [18] and proposes a complete group delay formula to elaborate the wave transmission behavior not only in a single-FP system but also in the complicated cascaded-FP structure without loss of generality. The total transmission group delay is decomposed into the dwell time (excluding the dispersion effect at the boundaries) and the boundary dispersive time. Dwell time depicts the time differences between the field energy stored in and escaping out of the intracavity region, covering the total group delay proposed in Ref. [18]. Boundary dispersive time is retrieved in the present paper to supplement the completeness of Ref. [18]. It originates from the "frequency-dependent" boundary reflection and transmission coefficients, describing an effective delay for a wave packet reflected and transmitted at the boundaries during the multiple-reflection stage. The GD decomposition clearly demonstrates that the round-trip destructive interference significantly reduces the field energy stored in the FP cavity, and thus decreases the cavity lifetime. It implies that the suppression of storage field energy by multiple-reflection interference serves as the third mechanism to realize superluminal delays, complementing the mechanisms of tunneling and anomalous dispersion.

A proof-of-principle experiment was conducted in a geometrically discontinuous waveguide system that forms a multiple-reflection FP interferometer. A broadband superluminality was observed (transmitting length = 11.000 mm, group delay $=8.43 \pm 1.24$ ps <36.69 ps). Moreover, two proposed time constituents of total transmission group delay could be retrieved by measuring the boundary reflection and transmission characteristics. It shows a very good agreement between the experimental results and theoretical predictions.

On the basis of single-FP-cavity analysis, an enhanced superluminality was experimentally demonstrated in a cascaded-FP system with an overall transmitting length of 30.000 mm, which yielded a group delay = 10.45 ± 1.49 ps, nearly an order of magnitude shorter than the luminal delay of 100.07 ps. The boundary dispersive time plays an important role in such a cascaded system, governing the wave transmission behaviors under off-resonant interference conditions.

This study lays the ground work for comprehending the slow-light effect and the superluminal behavior in multi-FP systems, and leads to a better understanding of controlling group delay with possible applications in signal transmission

*thschang@phys.nthu.edu.tw
†arrays@umich.edu

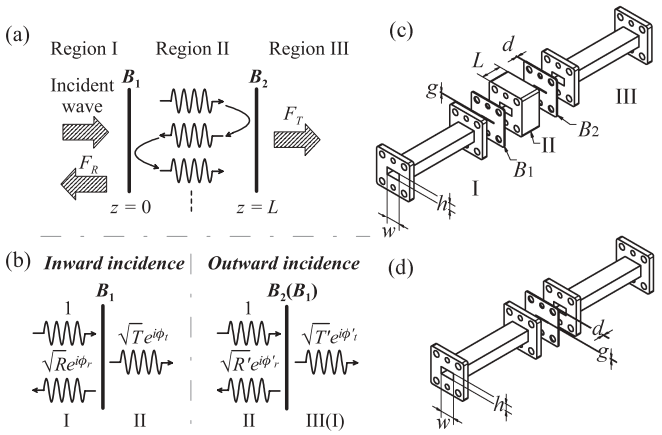

FIG. 1. (a) Schematic of a single-FP system, where B_1 and B_2 represent the first and second reflective boundaries, respectively. (b) Schematics of inward incidence and outward incidence. (c) A 3D geometrically discontinuous waveguide system, resembling a single-FP cavity [Fig. 1(a)]. Here, $w = 7.112$ mm (WR-28 waveguide), $h = 3.556$ mm, $g = 0.445$ mm, $d = 0.500$ mm, and $L = 10.000$ mm. (d) Closeup figure of the iris reflective boundary (B_1 and B_2) employed in (c).

[19] and wave packet switching for all-optical communication [20].

II. GROUP DELAY THEORY FOR SINGLE-FP SYSTEM

A single-FP system with three sections is employed for analysis as depicted in Fig. 1(a). Region I (input) is assumed to be identical to region III (output), and region II is embedded in between. Two reflective boundaries are formed at the interfaces of the adjacent regions. Figure 1(b) describes the inward-wave incidence from region I to II and outward-wave incidence from region II to region III or I.

A general expression for the group delay experienced by a wave packet as it traverses through a FP cavity (or barrier) has been obtained by Winful [17]:

$$\tau_g^T = \frac{\langle U\rangle}{P_{\rm in}} + \frac{{\rm Im}[F_R]}{k_0}\left(\frac{k_0}{\omega} - \frac{dk_0}{d\omega}\right).$$

Here, $\langle U\rangle$ is the time-averaged stored energy in the region II occupied by the cavity, $P_{\rm in}$ is the input power, F_R is the overall reflected field at region I, k_0 is the propagation constant in regions I and III, and ω is the frequency of the electromagnetic wave. The first term is known as the dwell time and represents the lifetime of stored energy in the central region (II) that acts as a cavity, where the field undergoes multiple reflections. The second term also contains the effects of multiple reflections through F_R as well as the dispersion effect. This term has been called a self-interference delay in Ref. [17]. However, in this form its physical significance is difficult to elucidate and it is also not clear how it lends itself to independent measurement. When specialized to a single-Fabry-Pérot system with dispersionless boundaries of intensity reflectivity R', the second term disappears and the group delay becomes identically equal to the dwell time under quasistatic conditions, which is given by [18]

$$\tau_g^T = \tau_d = \left[\frac{1-R'^2}{1+R'^2-2R'\cos(2kL)}\right]\frac{L}{v_{g\rm II}},$$

where $v_{g\rm II} \equiv d\omega/dk$, and k is the propagation constant in region II.

In order to clarify the role of the so-called self-interference term, Yao and Chang included the effects of dispersion at the reflective boundaries and generalized the simple FP result in a form that allows the independent measurement of each term in the expression. In what follows, we outline the group delay decomposition theory and describe an experiment that allows the direct measurement of each term.

As a wave encounters a boundary [Fig. 1(a)], it is partially reflected and partially transmitted, forming the reflected and transmitted waves that, jointly with the incident wave, satisfy the boundary conditions. In the inward incidence (from region I), $\sqrt{R}$ ($\sqrt{T}$) and ϕ_r (ϕ_t) describe the magnitude and the phase of the reflected (transmitted) wave, while $\sqrt{R'}e^{i\phi'_r}$ and $\sqrt{T'}e^{i\phi'_t}$ denote the reflected and transmitted waves in the case of outward incidence (from region II). The injected signal subsequently bounces back and forth between two reflective boundaries, thus creating a cavity field after the multiple reflections. The overall transmitted (reflected) signals in steady state [F_T (F_R)] result from the superposition of all multiple-reflection waves with different numbers of round-trip bounces and are given by

$$F_T \equiv |F_T|e^{i\varphi_T} = \frac{\sqrt{T}\times\sqrt{T'}}{\sqrt{1-2R'\cos(2\phi'_r+2kL)+R'^2}}e^{i\varphi_T}, \tag{1a}$$

$$\varphi_T = \phi_t + \phi'_t + kL + \tan^{-1}\left[\frac{R'\sin(2kL+2\phi'_r)}{1-R'\cos(2kL+2\phi'_r)}\right], \tag{1b}$$

$$F_R \equiv |F_R|e^{i\varphi_R} = \sqrt{R+2\sqrt{R}\sqrt{R'}|F_T|\cos(\phi'_r-\phi_r+kL+\varphi_T)+R'|F_T|^2}e^{i\varphi_R}, \tag{1c}$$

$$\varphi_R = \tan^{-1}\left[\frac{\sqrt{R}\sin(\phi_r)+\sqrt{R'}|F_T|\sin(kL+\phi'_r+\varphi_T)}{\sqrt{R}\cos(\phi_r)+\sqrt{R'}|F_T|\cos(kL+\phi'_r+\varphi_T)}\right], \tag{1d}$$

where k is the wave propagation constant in region II.

The transmission group delay (τ_g^T) describes the time difference between the time when the peak of the incident wave packet encounters the first boundary and the time when the peak of the output wave packet leaves the second boundary [21]. According to the stationary phase approximation (quasistatic condition) [15–18], $\tau_g^T = d\varphi_T/d\omega$. From Eq. (1b), τ_g^T is derived as follows.

$$\tau_g^T = \left[\frac{1-R'^2}{1-2R'\cos(2k_{\rm eff}L)+R'^2}\right]\left(\frac{L}{v_{g\rm II}}\right) + \frac{d\phi_t}{d\omega} + \left(2\frac{d\phi_r'}{d\omega}\right)\left[\frac{R'\cos(2k_{\rm eff}L)-R'^2}{1-2R'\cos(2k_{\rm eff}L)+R'^2}\right] + \frac{d\phi_t'}{d\omega} + \left[\frac{\sin(2k_{\rm eff}L)}{1-2R'\cos(2k_{\rm eff}L)+R'^2}\right]\left(\frac{dR'}{d\omega}\right), \quad (2)$$

where $k_{\rm eff} = k + \phi_r'/L$ and $v_{g\rm II} = d\omega/dk$.

Whenever the multiple-reflection wave travels a round trip between the two boundaries, it acquires a round-trip phase change of $2k_{\rm eff}L$, which has contributions from the wave propagation ($2kL$) and boundary effect ($2\phi_r'$). This phase shift determines the nature of the interference conditions between multiple-reflection components. The τ_g^T can be discussed in two special cases. One is the on-resonant condition occurring when $2k_{\rm eff}L = 2m\pi$, where m is an integer. The transmission group delay becomes

$$\tau_g^{T(\rm on)} = \left(\frac{1+R'}{1-R'}\right)\left(\frac{L}{v_{g\rm II}}\right) + \frac{d\phi_t}{d\omega} + \left(2\frac{d\phi_r'}{d\omega}\right)\left(\frac{R'}{1-R'}\right) + \frac{d\phi_t'}{d\omega}. \quad (3)$$

Under this condition, one reflected wave constructively interferes with the next one that experiences one more round-trip bounce. The other is the off-resonant condition at $2k_{\rm eff}L = (2m+1)\pi$, corresponding to destructive interference, and then τ_g^T equals

$$\tau_g^{T(\rm off)} = \left(\frac{1-R'}{1+R'}\right)\left(\frac{L}{v_{g\rm II}}\right) + \frac{d\phi_t}{d\omega} - \left(2\frac{d\phi_r'}{d\omega}\right)\left(\frac{R'}{1+R'}\right) + \frac{d\phi_t'}{d\omega}. \quad (4)$$

The first term in Eq. (2) is defined as the dwell time (τ_d) [17,18]:

$$\tau_d = \left[\frac{1-R'^2}{1-2R'\cos(2k_{\rm eff}L)+R'^2}\right]\left(\frac{L}{v_{g\rm II}}\right). \quad (5)$$

It represents the lifetime of stored field energy escaping through both ends (B_1 and B_2) of the FP cavity, assuming there is no dispersion in the boundary reflection and transmission coefficients. Equation (5) can be further expressed as

$$\tau_d = \tau_{d0} + (2\tau_{d0})f_{\rm MR}, \quad (6a)$$

$$f_{\rm MR} = \frac{R'\cos(2k_{\rm eff}L)-R'^2}{1-2R'\cos(2k_{\rm eff}L)+R'^2}, \quad (6b)$$

where $\tau_{d0} = L/v_{g\rm II}$ is a single-pass transit time and $f_{\rm MR}$ represents a multiple-reflection factor. The interference effect from multiple reflections manifests in $2\tau_{d0}f_{\rm MR}$, which can either lengthen or shorten the overall dwell time by changing $f_{\rm MR}$ to modulate the amount of stored energy under different round-trip phase change ($2k_{\rm eff}L$).

As $R' \to 0$, $f_{\rm MR}$ ($\propto R'$) turns into zero indicating the complete transmittance [$|F_T| \to 1$, Eq. (1a)], and then $\tau_d \to \tau_{d0}$. When $R' \to 1$, the effects of multiple reflections on dwell time are most clearly seen under on-resonant and off-resonant conditions. At the on-resonant state, $\tau_d^{\rm on} = (1+R')/(1-R')\tau_{d0}$ [first term in Eq. (3)]; the injected wave is strongly trapped between the two boundaries; hence $\tau_d^{\rm on}$ increases dramatically as R' increases, enhancing the slow-light effect. Under off-resonant conditions, $\tau_d^{\rm off} = (1-R')/(1+R')\tau_{d0}$ [first term in Eq. (4)]; most of the incident wave is reflected due to destructive interference that significantly reduces the stored field energy within the cavity. Since the dwell time is proportional to this stored energy [18], it will have a rather small value under off-resonant conditions. Consequently, the dwell time τ_d becomes relatively small at the condition of $R' \to 1$ with off-resonant operation [$2k_{\rm eff}L = (2m+1)\pi$], facilitating the apparent superluminal effect. However, this short dwell time must not be construed as a pulse propagating time from $z = 0$ to L as it is the consequence of superposition of multiple round-trip traveling waves, establishing a cavity field that then decays. The observed superluminality therefore satisfies causality if one recognizes that at least one round-trip propagation of the wave front was needed to establish the interference required for off-resonant transmission.

The remaining four terms in Eq. (2) jointly yield the boundary effects due to dispersion in the amplitude and phase of the boundary reflection and transmission coefficients, providing a "boundary dispersive time (τ_b)." The main contribution to τ_b comes from the frequency-dependent phase changes and can be expressed as

$$\tau_\phi = \frac{d\phi_t}{d\omega} + \left(2\frac{d\phi_r'}{d\omega}\right)\left[\frac{R'\cos(2k_{\rm eff}L)-R'^2}{1-2R'\cos(2k_{\rm eff}L)+R'^2}\right] + \frac{d\phi_t'}{d\omega}, \quad (7a)$$

$$\tau_\phi \equiv \tau_{\phi t} + 2\tau_{\phi r}f_{\rm MR} + \tau_{\phi t}, \quad (7b)$$

where $\phi_t = \phi_t'$ (by reciprocity), $\tau_{\phi t} \equiv d\phi_t/d\omega$, and $\tau_{\phi r} \equiv d\phi_r'/d\omega$. The first ($\tau_{\phi t}$) and last ($\tau_{\phi t}$) terms in Eq. (7a) are the transmission delays for a single pass through each boundary, while the second term ($2\tau_{\phi r}f_{\rm MR}$) represents the boundary reflection delay modified by the aforementioned multiple-reflection interference factor [$f_{\rm MR}$ in Eq. (6b)]. The contribution of the dispersion in boundary reflectivity (R') to τ_b is given by

$$\tau_R = \left[\frac{\sin(2k_{\rm eff}L)}{1-2R'\cos(2k_{\rm eff}L)+R'^2}\right]\left(\frac{dR'}{d\omega}\right). \quad (8)$$

For a single reflective boundary, a frequency-dependent reflectivity would normally result in pulse distortion but not change transmission group delay. However, in the presence of two boundaries and multiple reflections, the phases of the overall transmitted and reflected waves (φ_T and φ_R) depend on the reflectivity R' as shown in Eqs. (1b) and (1d), respectively. In other words, the interference between round-trip reflected waves for construction of final output

field leads to a contribution of reflectivity dispersion to the total group delay. Note that this contribution vanishes at the resonant and off-resonant interference conditions, while it could be enhanced through inserting material with anomalous dispersion [10,11] into the FP cavity.

The combination of τ_ϕ and τ_R forms the boundary dispersive time (τ_b) that is the result of accumulated time delays at the boundaries for a wave packet undergoing multiple reflections. Thus, τ_b explicitly describes the effective time for a narrow-band pulse spending on the two-sided boundaries of a FP system.

Finally, the total transmission group delay can be expressed as

$$\tau_g^T = \tau_d + \tau_b = \tau_d + \tau_\phi + \tau_R = (\tau_{d0} + 2\tau_{d0} f_{\mathrm{MR}}) + (2\tau_{\phi t} + 2\tau_{\phi r} f_{\mathrm{MR}}) + \tau_R. \quad (9)$$

III. EXPERIMENTAL DEMONSTRATION OF SUPERLUMINALITY IN SINGLE-FP SYSTEM

A geometrically discontinuous waveguide system with two reflective iris boundaries is introduced here [Fig. 1(c)] to demonstrate both subluminal ("slow-light") and superluminal ("fast-light") group delays based on the multiple-reflection mechanism. Regions I (input), II (propagating) and III (output) are identical WR-28 waveguides with width $w = 7.112$ mm and height $h = 3.556$ mm, while the two-sided symmetric irises (B_1 and B_2) are undersized waveguides with a greatly reduced height of $g = 0.445$ mm, and the same width w (7.112 mm). The cutoff frequency ($\omega_c = c\pi/a = 21.076 \times 2\pi$ Giga-rad/s) and propagation constant ($k = \sqrt{\omega^2 - \omega_c^2}/c$) of the operating mode (TE_{10}) are thus unchanged throughout the whole E-plane structure, making the system fundamentally different from that in the previous superluminal tunneling experiments [5–7,12,13]. The propagation length L and iris length d are respectively specified as 10.000 and 0.500 mm, satisfying the condition of $kd < 0.1\pi \ll kL$. This condition prevents intrinsic resonant behavior within a single iris and therefore ensures that the two-sided irises effectively perform like the clear-cut reflective boundaries (B_1 and B_2) depicted in Fig. 1(a).

The frequency-domain overall transmission and reflection coefficients [F_T and F_R as defined in Fig. 1(a)] are shown in Figs. 2(a) and 2(b) by blue triangles with error bars, measured by a performance network analyzer (PNA, Aglient Technologies E8363B). Based on the stationary phase approximation, the total group delay for a narrow-band pulse transmitted through this FP system [τ_g^T, blue triangles in Fig. 2(c)] can be directly derived by $d\varphi_T/d\omega$ from the measured phase information provided in Fig. 2(a). The gray dashed line in Fig. 2(c) represents the luminal group delay of $\tau_0 \equiv (L + 2d)/c = 36.69$ ps, i.e., the propagation delay for a wave packet making a single pass through a free space distance of $L + 2d$ with velocity c. Delays shorter than this are termed as "superluminal," whereas longer delays are referred to as "subluminal."

At frequencies equal to 27.609 and 38.014 GHz, on-resonant conditions occur with $2k_{\mathrm{eff}}L = 4\pi$ and 6π, leading to a maximum transmission of nearly 100% [Fig. 2(a)]. The group delays at these frequencies are 272.97 ± 0.17 ps ($7.440\tau_0$) and 470.22 ± 3.23 ps ($12.815\tau_0$), respectively. These subluminal delays would correspond to wave packets propagating with the slow-light velocities of $0.134c$ and $0.078c$, respectively, if the input and output envelope peaks were related by a simple causal translation over the distance $L + 2d$ (11.000 mm). A wide-band superluminality appearing from 29.317 to 36.753 GHz [the region below gray dashed line in Fig. 2(c), 22.51% bandwidth] is observed, in which the shortest group delay is only 8.43 ± 1.24 ps at 33.242 GHz ($2k_{\mathrm{eff}}L = 5\pi$), corresponding to the apparent faster-than-light delay of $0.230\tau_0$. The red curves in Figs. 2(a)–2(c) represent the simulation results obtained via a three-dimensional (3D) full-wave solver, high-frequency structure simulator (HFSS), which show a very good agreement with the experimental data.

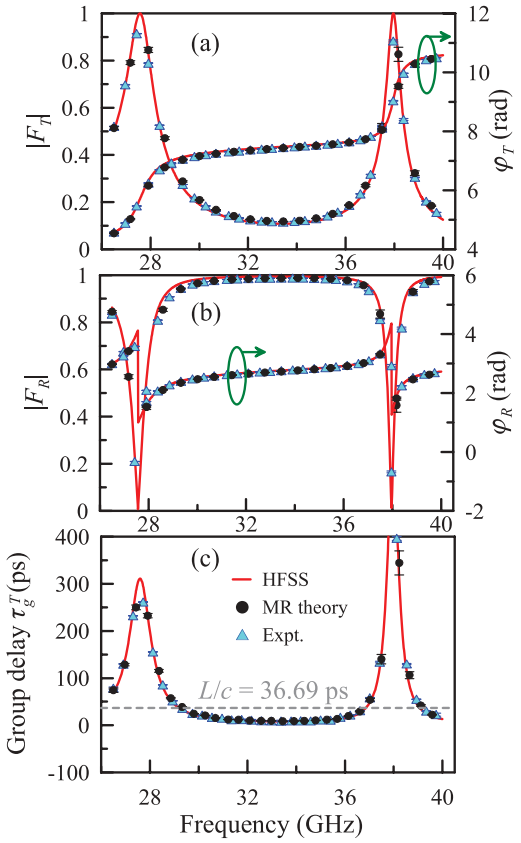

FIG. 2. (Color online) Total transmission coefficient (a), reflection coefficient (b), and transmission group delay (c) of the single-FP system. The blue (light gray) triangles are the measured data of an overall system depicted in Fig. 1(c), while the black dots represent the calculated results based on the proposed theory and the measured iris boundary characteristics (demonstrated in Fig. 3). The red (dark gray) curves are the simulation from HFSS.

To verify the proposed group delay decomposition [Eq. (9)], the wave reflection and transmission behaviors at a single-iris boundary [Fig. 1(d)] must be explicitly characterized due to their essential role in the multiple-reflection process. The reflection ($\sqrt{R'}e^{i\phi_r'}$) and transmission ($\sqrt{T}e^{i\phi_t}$) coefficients of a single iris are consequently measured and demonstrated in Figs. 3(a) and 3(b), respectively. The high boundary reflection rate ($|R'|$ up to about 0.8) and frequency-dependent boundary transmission and reflection phases ($\phi_t = \phi_t'$ and ϕ_r') originate

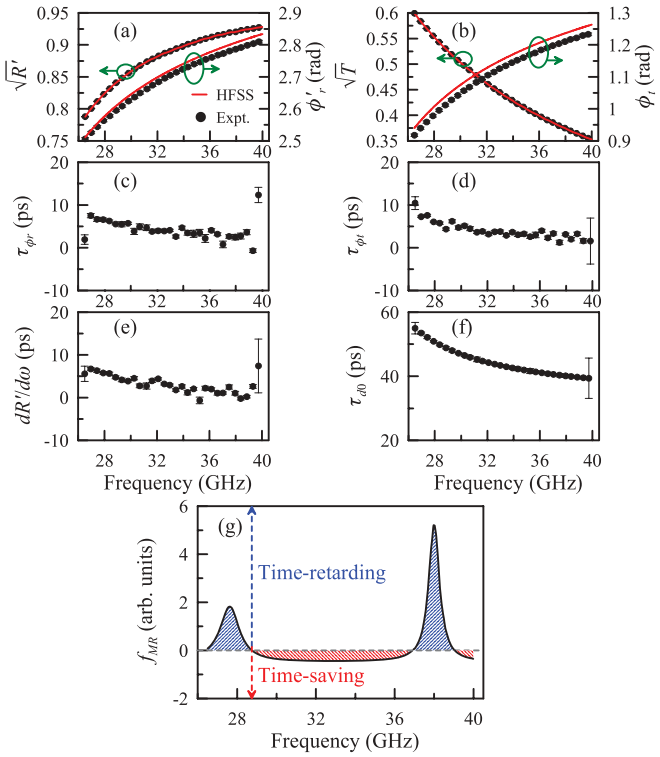

FIG. 3. (Color online) (a) The experimental results (black dots) of the outward-incident reflection coefficient ($\sqrt{R'}e^{i\phi_r'}$) and (b) transmission coefficient ($\sqrt{T}e^{i\phi_t}$) for individual iris reflective boundary delineated in Fig. 1(d). The red (dark gray) curves here are the HFSS simulation results. The time constituents of (c) $\tau_{\phi r}$ ($d\phi_r'/d\omega$), (d) $\tau_{\phi t}$ ($d\phi_t/d\omega$), and (e) $dR'/d\omega$ are derived from the measured characteristics of the iris boundary shown in (a) and (b). (f) The single-pass transit time τ_{d0} was measured with a uniform WR-28 waveguide, and (g) is the multiple-reflection factor (f_{MR}).

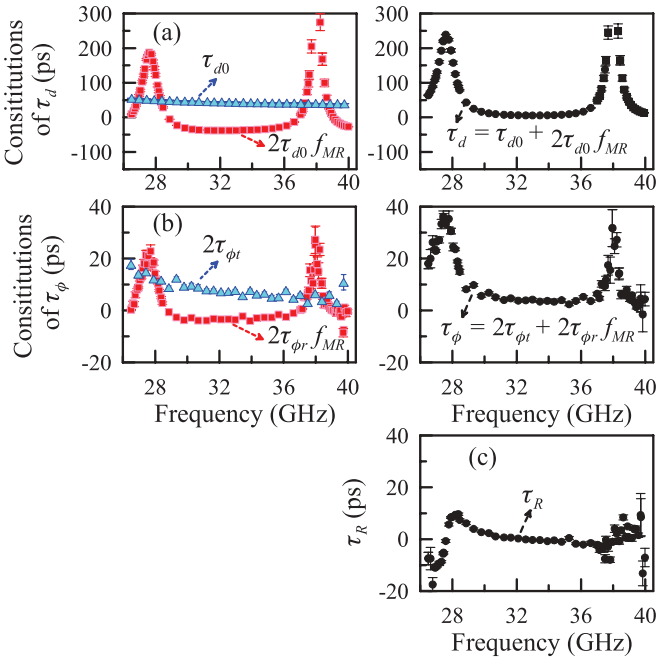

FIG. 4. (Color online) (a) Left-hand panel shows the τ_{d0} [blue (light gray) triangles] and $2\tau_{d0}f_{\mathrm{MR}}$ [red (dark gray) squares], which are the essentialities of dwell time (τ_d, black dots) illustrated in the right-hand panel. (b) The boundary transmission time [$2\tau_{\phi t}$, blue (light gray) triangles] and boundary reflection time [$2\tau_{\phi r}f_{\mathrm{MR}}$, red (dark gray) squares] are demonstrated on the left-hand panel, while the sum of these two delay times is τ_ϕ (right-hand panel). The delay time associated with the dispersion in boundary reflectivity (τ_R) is shown in (c).

from the strong modal effect occurring at the geometrically discontinuous structures [9,22].

Once $\sqrt{R'}e^{i\phi_r'}$ and $\sqrt{T}e^{i\phi_t}$ are well characterized, $\tau_{\phi r}(=d\phi_r'/d\omega)$ and $\tau_{\phi t}$ $(=d\phi_t/d\omega)$ can be subsequently calculated [shown in Figs. 3(c) and 3(d), respectively], representing the basic time delays for single-reflection and single-transmission events within an iris region. Figure 3(e) shows $dR'/d\omega$, which exhibits a frequency dependence similar to $\tau_{\phi r}$ and $\tau_{\phi t}$ in the present multiple-reflection system. On the other hand, the single-pass time delay for a wave packet traveling from one reflective boundary to the other [$\tau_{d0} = L/v_{g\mathrm{II}} = Ldk/d\omega$ shown in Fig. 3(f)] is directly measured from a uniform WR-28 waveguide with a propagating length $L = 10.000$ mm.

After a substitution of the measured $\sqrt{R'}e^{i\phi_r'}$ [Fig. 3(a)] into Eq. (6b), the multiple-reflection factor f_{MR} [Fig. 3(g)] is obtained, revealing the strong correlation to the extraordinary group delay in Fig. 2(c). Owing to the positive single-pass delays, i.e., $\tau_{\phi r}$ and τ_{d0} [Figs. 3(c) and 3(f)], the positive f_{MR} provides an enhancement effect, which increases τ_g^T and leads to the slow-light phenomena in the regions of 26.500–29.317 GHz and 36.753–39.224 GHz in Fig. 2(c). On the other hand, the negative f_{MR} corresponds to a suppression mechanism due to destructive interference, thus resulting in an ultrashort τ_g^T for broadband superluminal delays (from 29.317 to 36.753 GHz).

According to the group delay decomposition, the dwell time [τ_d, Fig. 4(a)], and the boundary dispersive time [$\tau_b = \tau_\phi + \tau_R$, Figs. 4(b) and 4(c)], can be further acquired by employing the measured iris boundary characteristics demonstrated in Fig. 3. The sum of τ_d, τ_ϕ, and τ_R gives the total group delay [Fig. 2(c), black dots], which perfectly matches with the measured data of the overall FP system [Fig. 2(c), blue triangles], as well as the simulation results [Fig. 2(c), red curve].

The τ_d [Fig. 4(a)] and the τ_ϕ [Fig. 4(b)] are linearly dependent on f_{MR} [Fig. 3(g)], while the τ_R [Fig. 4(c)] is relatively small in the present single-FP system due to the nearly dispersionless reflectivity (R') of the boundary. At the first on-resonant state (27.609 GHz), the positive f_{MR} of 1.811 makes τ_d achieve 239.07 ± 0.43 ps (consisting of $\tau_{d0} = 51.72 \pm 0.11$ ps and $2\tau_{d0}f_{\mathrm{MR}} = 187.35 \pm 0.33$ ps), thus contributing 87.58% of the total transmission group delay and dominating the slow-light phenomenon. In the vicinity of 29.317-36.753 GHz, $2\tau_{d0}f_{\mathrm{MR}}$ turns to a negative value of -37.63 ± 0.08 ps and cancels with τ_{d0} $(=43.14 \pm 0.07$ ps), thus resulting in a small τ_d of 5.51 ± 0.05 ps, much shorter than the light propagating time in vacuum over an equal traveling distance [$(L + 2d)/c = 36.69$ ps]. This ultrashort dwell time results from the fact that most of the incident signal is reflected in front of the FP system under a destructive-interference condition; hence only a small amount of field energy is injected into the intracavity region. The less the stored field energy

is, the shorter the dwell time will be for all stored energy escaping out of the cavity. If the boundary dispersive time ($\tau_b = \tau_\phi + \tau_R$) is likewise small, superluminal delays would be obtained.

During the off-resonant operation (33.242 GHz), the negative f_{MR} (–0.436) yields a negative $2\tau_{\phi r} f_{\mathrm{MR}}$ of -3.16 ± 0.23 ps, which counteracts the transmission time at two-sided boundaries ($2\tau_{\phi t}$, 5.97 ± 0.41 ps) to form a tiny τ_ϕ ($=2\tau_{\phi t} + 2\tau_{\phi r} f_{\mathrm{MR}}$) of 2.81 ± 0.41 ps. The τ_R in the vicinity of off-resonant interference is negligible (only -0.55 ± 0.06 ps) since it is proportional to $\sin(2k_{\mathrm{eff}}L) \to 0$ under off-resonant operation. An ultrashort boundary dispersive time (τ_b) ultimately indicates that the wave packet effectively spends less time at the boundaries.

The cancellations between τ_{d0} ($2\tau_{\phi t}$) and $2\tau_{d0} f_{\mathrm{MR}}$ ($2\tau_{\phi r} f_{\mathrm{MR}}$) make τ_d and τ_ϕ simultaneously drop far below $(L + 2d)/c = 36.69$ ps, resulting in the positive superluminality ($\tau_g^T = 7.77 \pm 0.42$ ps). The slight discrepancy between the calculated group delay from decomposition theory [7.77 ± 0.42 ps, the black dots in Fig. 2(c)] and the experimental result measured from the overall system [8.43 ± 1.24 ps, the blue triangles in Fig. 2(c)] could be well included and explained by the error bars.

The above experiment demonstrates how multiple-reflection interference in regions of allowed propagation results in a modulation of stored field energy and thus yields a frequency-dependent cavity lifetime. It should be noted that although the concept of a cavity lifetime is widely used in applications such as laser dynamics, there is always an unspoken assumption that the cavity is on resonance. By introducing the concept of a frequency-dependent cavity lifetime, we are able to explain the anomalously short group delays on the basis of the suppression of stored field energy below the cavity-free values by round-trip destructive interference. We have also elucidated the contribution of dispersion at the boundaries to the transmission magnitude and transmission group delay. It is believed that the boundary dispersion effect could be further enhanced through multiple-reflection interference. A cascaded-FP system with strong multiple reflections, revealing the significance of boundary dispersive time ($\tau_b = \tau_\phi + \tau_R$), is therefore discussed in the following to distinguish the physical meanings of the two decomposed time constituents.

IV. GROUP DELAY AND THE GENERALIZED HARTMAN EFFECT IN CASCADED-FP CAVITIES

A cascaded-FP waveguide system (Fig. 5) consists of two identical single-FP cavities [C_{I} and C_{III} defined in Fig. 1(c)] jointly connected by a bridge (WR-28 waveguide) with length $L_m = 8.000$ mm, which forms another cavity (C_{II}) embedded between C_{I} and C_{III}. The measured overall transmission coefficient denoted by $|F_T^c|e^{i\varphi_T^c}$ and the transmission group delay ($\tau_g^{Tc} = d\varphi_T^c/d\omega$) of this cascaded-FP system are depicted in Figs. 6(a) and 6(b) by blue triangles.

The wave behaviors in this FP system can be explicitly described by an effective two-boundary model graphically depicted in Fig. 5(b). Cavities C_{I} and C_{III} are effectively equivalent to two artificial boundaries (B_{e1} and B_{e2}), the characteristics of which are therefore completely determined by the wave transmission and reflection properties at individual

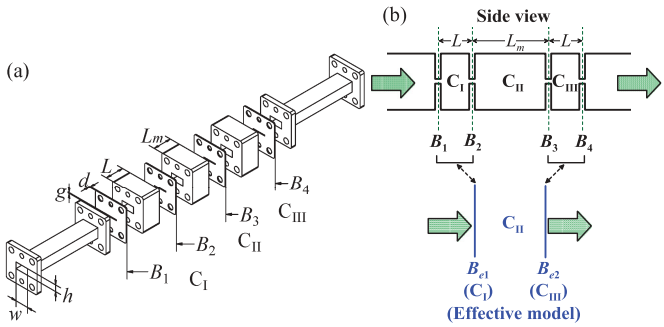

FIG. 5. (Color online) (a) Schematic of cascaded-FP system in waveguide system, where $L = 10.000$ mm and $L_m = 8.000$ mm. Notably, the two-sided cavities (C_{I} and C_{III}) are identical to the single-FP system specified at Fig. 1(c). (b) An effective two-boundary model ($B_{e1} + C_{\mathrm{II}} + B_{e2}$) equivalent to the original four-boundary cascaded-FP system ($B_1 + C_{\mathrm{I}} + B_2 + C_{\mathrm{II}} + B_3 + C_{\mathrm{III}} + B_4$).

single-FP cavity [Fig. 1(c)]. The transmission rate ($\equiv T_{\mathrm{eff}}$) and transmission group delay ($\equiv \tau_{g\,\mathrm{eff}}^T$) of both effective boundaries are thus equal to $|F_T|^2$ and $\tau_g^T = d\varphi_T/d\omega$, while the reflection rate ($\equiv R_{\mathrm{eff}}$) and reflection group delay ($\tau_{g\,\mathrm{eff}}^R$) should be $|F_R|^2$ and $\tau_g^R = d\varphi_R/d\omega$. These four critical parameters ($|F_T|^2$, τ_g^T, $|F_R|^2$, and τ_g^R) have been defined in the case of a single-FP cavity [Fig. 1 and Eq. (1)] and are clearly characterized in Fig. 2.

According to the single-FP model proposed in Sec. II, the total transmission group delay in the cascaded-FP system (τ_g^{Tc}) can be derived by employing Eq. (9) with the

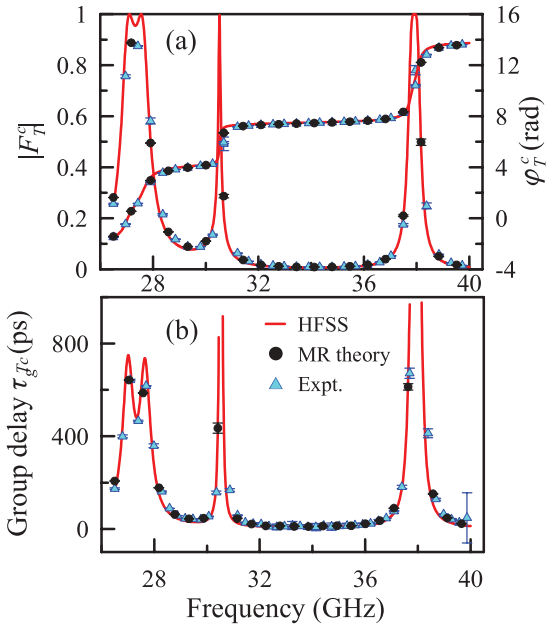

FIG. 6. (Color online) Total transmission coefficient (a) and transmission group delay (b) of the cascaded-FP system. The measured data of an overall system are presented in blue (light gray) triangles, while the black dots represent the calculated results based on the GD decomposition theory with substitution of the measured characteristics of the single-FP cavity shown in Fig. 2. The red (dark gray) curves are the simulations from HFSS.

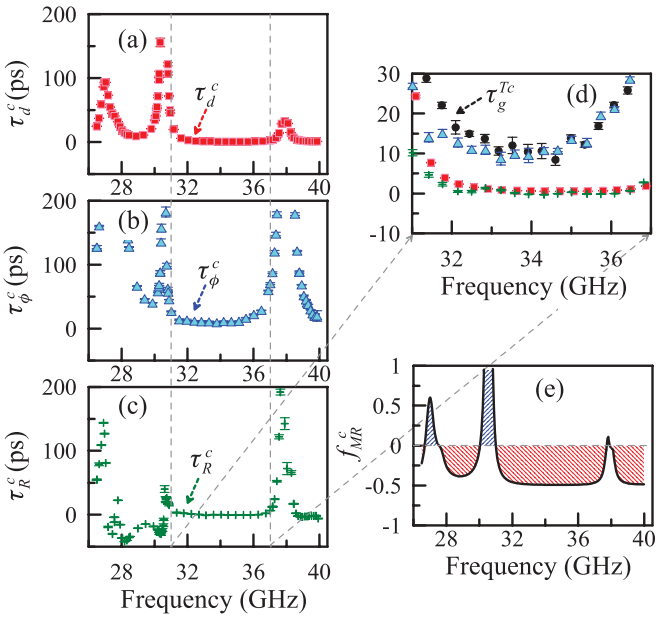

FIG. 7. (Color online) (a) τ_d^c [red (dark gray) squares], (b) τ_ϕ^c [blue (light gray) triangles], and (c) τ_R^c (green crosses). A closeup figure of (a)–(c) at the single-FP off-resonant region (31–37 GHz) is demonstrated in (d), in which the black dots represent the total transmission group delay ($\tau_g^{Tc} = \tau_d^c + \tau_\phi^c + \tau_R^c$). (e) The multiple-reflection factor ($f_{\rm MR}^c$) of this cascaded-FP system.

substitutions $L \to L_m$, $\tau_{d0} \to L_m/v_{g\rm II}$, $\tau_{\phi t} \to \tau_{g\,\rm eff}^T = d\varphi_T/d\omega$, $\tau_{\phi r} \to \tau_{g\,\rm eff}^R = d\varphi_R/d\omega$, and $R' \to R_{\rm eff} = |F_R|^2$, which yields

$$\tau_g^{Tc} = \tau_d^c + \tau_b^c = \tau_d^c + \tau_\phi^c + \tau_R^c = \left[\frac{L_m}{v_{g\rm II}} + \left(2\frac{L_m}{v_{g\rm II}}\right) f_{\rm MR}^c\right] + \left[2\frac{d\varphi_T}{d\omega} + \left(2\frac{d\varphi_R}{d\omega}\right) f_{\rm MR}^c\right] + \tau_R^c, \quad (10a)$$

$$f_{\rm MR}^c = \frac{|F_R|^2 \cos\left(2k_{\rm eff}^c L_m\right) - |F_R|^4}{1 - 2|F_R|^2 \cos\left(2k_{\rm eff}^c L_m\right) + |F_R|^4}, \quad (10b)$$

$$\tau_R^c = \left[\frac{\sin\left(2k_{\rm eff}^c L_m\right)}{1 - 2|F_R|^2 \cos\left(2k_{\rm eff}^c L_m\right) + |F_R|^4}\right]\left(\frac{d|F_R|^2}{d\omega}\right), \quad (10c)$$

where $k_{\rm eff}^c \equiv k + \varphi_R/L_m$.

The superscript "c" denotes the decomposed delay times associated with the cascaded-FP system, the frequency responses of which are explicitly illustrated in Fig. 7. Furthermore, the sum of τ_d^c, τ_ϕ^c, and τ_R^c gives the total group delay [black dots in Fig. 6(b)], which has a very good agreement with the experimental (blue triangles) and simulation (red curve) results.

In the vicinity of the single-FP off-resonance region (e.g., 33.242 GHz), the group delay is 10.45 ± 1.49 ps (τ_g^{Tc}) over a cascaded-transmission length of $2L + 4d + L_m = 30.000$ mm. The group delay for light propagating through an equal distance in free space would be 100.07 ps, and thus we have nearly an order of magnitude enhancement in the apparent "group velocity," achieving 28.7×10^8 m/s. We stress, of course that nothing is actually propagating with such velocity inside the cavity and that the group delay here is actually an off-resonance cavity lifetime. By comparison, the superluminal group delay in the single-FP system with a shorter transmission distance of $L + 2d = 11.000$ mm is 8.43 ± 1.24 ps [Fig. 2(c)], implying an apparent group velocity of 13.05×10^8 m/s, about half that of the cascaded system. The enhancement of apparent superluminality in the cascaded-FP system over the single-FP structure could be explicitly interpreted through the relation between dwell time [$\tau_d^c = (1 + 2f_{\rm MR}^c)L_m/v_{g\rm II}$, red squares in Fig. 7(a)] and boundary dispersive time [$\tau_b^c = \tau_\phi^c + \tau_R^c$, with $\tau_\phi^c (= 2\tau_g^T + 2\tau_g^R f_{\rm MR}^c)$ shown in blue triangles in Fig. 7(b), and τ_R^c illustrated in the green crosses in Fig. 7(c)]. These decomposed components are calculated from Eq. (10) based on the measured characteristics of an individual single-FP cavity specified in Fig. 2. The dwell time (τ_d^c) represents the time delay for the signal staying within the middle cavity ($C_{\rm II}$), while the boundary dispersive time (τ_b^c) describes the effective time accumulated from transmission ($\propto 2\tau_g^T$) and reflection ($\propto 2\tau_g^R$) delays at the effective dispersive boundaries B_{e1} and B_{e2}, i.e., the first and the third cavities ($C_{\rm I}$ and $C_{\rm III}$).

During the off-resonance operation of a single-FP cavity (for instance, 33.242 GHz), the reflectivity of the effective boundaries [B_{e1} ($C_{\rm I}$) and B_{e2} ($C_{\rm III}$)] are quite high [$R_{\rm eff} = |F_R|^2 \approx 1 - |F_T|^2 \to 98\%$; refer to Fig. 3(a)] due to the destructive interference. The incident signals would be almost totally reflected at the first cavity ($C_{\rm I}$) and therefore only a rather small part can be transmitted into $C_{\rm II}$. The stored energy in the intracavity region ($C_{\rm II}$) is thus greatly reduced, implying an ultrashort dwell time (τ_d^c) as shown in Figs. 7(a) and 7(d). In other words, the wave packet spends most of the time delay for reflection at the first effective boundary, i.e., the cavity $C_{\rm I}$, which explains why τ_g^{Tc} (10.45 ± 1.49 ps) has a large contribution from τ_ϕ^c [8.73 ± 1.60 ps, $\tau_\phi^c/\tau_g^{Tc} = 83.54\%$ in Figs. 7(b) and 7(d)]. Notably, the τ_R^c [Figs. 7(c) and 7(d)] is still negligible at 33.242 GHz due to the nearly dispersionless boundary reflectivity ($|F_R|^2$) ranging between 29.317 and 36.753 GHz. We can conclude that boundary dispersive time ($\tau_b^c = \tau_\phi^c + \tau_R^c \sim \tau_\phi^c$) fully dominates the transmission group delay (τ_g^{Tc}) in such a cascaded-FP system under off-resonant operation due to the strong suppression of dwell time (τ_d^c), as well as the stored field energy by high boundary reflectivity.

From the mathematical perspective, the multiple-reflection factor [$f_{\rm MR}^c$ defined in Eq. (10b) and shown in Fig. 7(e)] will be reduced to $-\frac{1}{2}$ under the case of extremely high boundary reflectivity ($R_{\rm eff} = |F_R|^2 \to 1$). Meanwhile, the dwell time in region II is reduced to zero [$\tau_d^c \propto (1 + 2f_{\rm MR}^c) \to 0$], and thus the importance of boundary dispersive time ($\tau_b^c \sim \tau_\phi^c$) markedly increases, completely in contrast to the situation in a single-FP system. The length of the middle cavity (L_m) now certainly becomes an irrelevant parameter for τ_d^c, as well as τ_ϕ^c, because the constant $f_{\rm MR}^c (= -1/2)$ is essentially independent of L_m. Therefore, the longer the L_m is, the faster the "apparent group velocity" [$v_{g\,\rm eff}^c \sim (2L + 4d + L_m)/\tau_\phi^c \propto L_m$] that will be observed in the cascaded-FP system. This lack of dependence of the group delay on the length in a region of allowed propagation has been called the "generalized Hartman effect" [6]. However, as pointed out by Winful [18], this is just a trivial artifact arising from the fact that there is no energy in the region to be transmitted due to extremely high boundary reflectivity. The generalized Hartman effect does not exist. If energy survives into the middle region ($C_{\rm II}$), its delay time will

increase linearly with L_m in the same manner as the case of a single-FP system with low boundary reflection rate.

V. CONCLUSION

In summary, multiple-reflection interference leading to the enhancement and the suppression of intracavity stored field energy has been demonstrated to induce subluminal and superluminal delays in FP systems without tunneling and anomalous-dispersion regions. Previous work is generalized to include the effect of dispersion at the FP boundaries by a boundary dispersive time, which represents the accumulated delay spending on the boundaries, in addition to the signal dwell time staying inside the intracavity region. These two constituents can be independently measured in experiment and jointly describe the total transmission group delay. The experimental results show excellent agreement with the theoretical predictions for both single-Fabry-Pérot and cascaded-Fabry-Pérot systems.

ACKNOWLEDGMENTS

This work was sponsored by the National Science Council of Taiwan under Contract No. NSC 101-2112-M-007-005-MY3. The authors appreciate technical support from Ansys Inc.

[1] L. Thevenaz, Nat. Photonics **2**, 474 (2008).
[2] M. D. Stenner, D. J. Gauthier, and M. A. Neifeld, Phys. Rev. Lett. **94**, 053902 (2005).
[3] D. R. Solli, C. F. McCormick, C. Ropers, J. J. Morehead, R. Y. Chiao, and J. M. Hickmann, Phys. Rev. Lett. **91**, 143906 (2003).
[4] H. G. Winful, New J. Phys. **8**, 101 (2006).
[5] A. M. Steinberg, P. G. Kwiat, and R. Y. Chiao, Phys. Rev. Lett. **71**, 708 (1993).
[6] S. Longhi, P. Laporta, M. Belmonte, and E. Recami, Phys. Rev. E **65**, 046610 (2002).
[7] Ch. Spielmann, R. Szipocs, A. Stingl, and F. Krausz, Phys. Rev. Lett. **73**, 2308 (1994).
[8] T. E. Hartman, J. Appl. Phys. **33**, 3427 (1962).
[9] H. Y. Yao and T. H. Chang, Prog. Electromagn. Res. **122**, 1 (2012).
[10] M. D. Stenner, D. J. Gauthier, and M. A. Neifeld, Nature **425**, 695 (2003).
[11] L. J. Wang, A. Kuzmich, and A. Dogariu, Nature **406**, 277 (2000).
[12] A. Enders and G. Nimtz, Phys. Rev. B **47**, 9605 (1993).
[13] G. Nimtz, A. Haibel, and R.-M. Vetter, Phys. Rev. E **66**, 037602 (2003).
[14] H. G. Winful, Opt. Express **10**, 1491 (2002).
[15] H. G. Winful, Phys. Rev. Lett. **90**, 023901 (2003).
[16] H. G. Winful, Phys. Rev. Lett. **91**, 260401 (2003).
[17] H. G. Winful, Phys. Rev. E **68**, 016615 (2003).
[18] H. G. Winful, Phys. Rev. E **72**, 046608 (2005); **73**, 039901(E) (2006).
[19] M. Xin, F. Yin, C. Lei, M. Chen, H. Chen, C. Tang, and S. Xie, Opt. Lett. **35**, 1596 (2010).
[20] S. Manipatruni, P. Dong, Q. Xu, and M. Lipson, Opt. Lett. **33**, 2928 (2008).
[21] R. Landauer and Th. Martin, Rev. Mod. Phys. **66**, 217 (1994).
[22] H. Y. Yao and T. H. Chang, Prog. Electromagn. Res. **101**, 291 (2010).